Structural differences between the closed and open states of channelrhodopsin-2 as observed by EPR spectroscopy

Nils Krause[‡], Christopher Engelhard[‡], Joachim Heberle, Ramona Schlesinger[*], Robert Bittl[*]

Freie Universität Berlin, Fachbereich Physik, Arnimallee 14, 14195 Berlin, Germany

[‡] These authors contributed equally.
[*] to whom correspondence should be addressed:
Robert Bittl (robert.bittl@fu-berlin.de)
Ramona Schlesinger (r.schlesinger@fu-berlin.de)

Abstract
Channelrhodopsin is a cation channel with the unique property of being activated by light. To address structural changes of the open state of the channel, two variants which contain either 1 or 2 wild-type cysteines were derivatized with nitroxide spin label and subjected to electron paramagnetic resonance spectroscopy. Both variants contained the C128T mutation to trap the long-lived P_3^{520} state by illumination. Comparison of spin-spin distances in the dark state and after illumination reflect conformational changes in the conductive P_3^{520} state involving helices B and F. Spin distance measurements reveal that channelrhodopsin forms a dimer even in the absence of intermolecular N-terminal cysteines.

Abbreviations
ChR2, channelrhodopsin 2; SRII, sensory rhodopsin II; BR, bacteriorhodopsin; EPR, electron paramagnetic resonance; *cw*-EPR, continuous wave electron paramagnetic resonance; pELDOR, pulsed electron-electron double resonance; DEER, double electron-electron resonance; MTSL, (1-oxyl-2,2,5,5-tetramethylpyrroline-3-methyl)methanethiosulfonate spin label; MES, 2-(N-morpholino)ethanesulfonic acid; DM, decyl-ß-D-maltoside

Keywords
Optogenetics, rhodopsin, light-activated cation channel, photocycle, membrane protein, EPR spectroscopy

Highlights
We find specific dimerization independent of cysteine residues
ChR2 shows a structural change in helix F upon light excitation as in other retinal proteins
- We find additional structural changes in either helix B or the dimerization interface

Introduction

Shortly after the demonstration of light-gated cation channel activity [1] channelrhodopsin-2 (ChR2) has received enormous attention as a tool for neurophysiologists to optically trigger action potentials and other cellular activities [2]. After flash-photolytic and electrophysiological characterization of ChR2 from *Chlamydomonas reinhardtii*, IR difference spectroscopy indicated large structural changes in the protein backbone in various intermediate states [3,4] as well as a proton release and uptake event in the course of the photocycle [5]. The recently published structure of a ChR1/ChR2 (C1C2) hybrid variant [6] (Fig. 1) resolved at a resolution of 2.3 Å, displayed the overall arrangement of channelrhodopsin and provides a basis for probing structural changes at different positions during channel activity. However, structural insight into the activation of the channel upon photo-excitation of the chromophore is lacking so far.

Conformational changes are here studied by site-directed spin labeling in conjunction with EPR spectroscopy. Pulsed Electron Double Resonance (pELDOR) spectroscopy [7] provides precise distance measurements between spin label sites in the 1.8–6 nm range with sub-nm precision [8]. In microbial rhodopsins like the proton pump bacteriorhodopsin (BR) and the sensory rhodopsin II (SRII), the light-dependent movement of helix F has been detected using EPR techniques [9-11]. Tilting of helix F in SRII induces conformational changes in the cognate transducer II to convey the light signal to the downstream components of the phototactic signal cascade [12]. Visual, vertebrate rhodopsin, belonging to the G-protein-coupled receptors, shows similar helix F shifts monitored by EPR spectroscopy [8,13-15], indicating a general action mechanism of retinal proteins.

For this study two ChR2 variants, exhibiting delayed open states, were designed to test for helix F displacements from the dark state to the conducting state. Wild-type ChR2 has nine native cysteines which compete for labeling depending on their accessibility. Our ChR2 variants have only one (C79) and two (C79, C208) native cysteines remaining, respectively. These variants enable site directed labeling on cysteine positions with the thiol-selective spin label (1-oxyl-2,2,5,5-tetramethylpyrroline-3methyl)methanethiosulfonate (MTSL). C79 is in the loop connecting helix A and B, adjacent to helix B whereas C208 is positioned at the intercellular end of helix F. By substitution of C128 with threonine [16,17] the variants were engineered in a way that the photocycle intermediate P_3^{520}, the conducting state, is accumulated upon illumination, in contrast to the wild-type, which accumulates P_4^{480}, a desensitized state wothout ion conductance [18]. Since the yeast *Pichia pastoris* has been shown to express sufficient amounts of ChR2 for biophysical studies [18], both variants were produced in this host, spin labeled, the activity validated by FTIR spectroscopy, and subjected to pELDOR measurements before and after illumination.

Materials and Methods

Construction of recombinant ChR2 and purification

The ChR2 variant containing mutations C34,36,87,179,183,259A and C128T but retaining wild-type cysteines 79 and 208 is abbreviated as ChR2-C79/208. A variant further reduced in cysteine 208 is named ChR2-C79. The variants were generated with oligonucleotide-directed mutagenesis using PCR. The recombinant ChR2 sequences (coding for aa residues 1-307 of ChR2 and a 10x His-tag) were inserted into the EcoRI/NotI site of pPIC9K (Invitrogen) to generate a fusion to the alpha factor signal sequence of the vector. Variants ChR2-C79/208 and ChR2-C79 were heterologously expressed in the yeast *Pichia pastoris* strain SMD 1163 as

described in Bamann *et al.* [17]. For purification the cells were cracked at 2.7 kbar in a cell disruptor (Constant Systems, 1.1kW). The membranes with ChR2 were harvested at 186000g for 2-3 h and solubilized in 20 mM MES (pH 6), 100 mM NaCl, 2 M urea, 1% (w/v) DM (Glycon Biochemicals) overnight at 4°C. The insoluble fraction was removed by ultracentrifugation for 1.5 h at 186000g and 4°C. The supernatant was blended with 120 mM imidazole (final concentration) and loaded onto a Ni-NTA sepharose column in an ÄktaTM avant system (GE Healthcare). After two washing steps with 60 and 120 mM imidazole a linear imidazole gradient from 60 to 500 mM was applied. ChR2 containing fractions were pooled and concentrated with Amicon concentrators (50 kDa exclusion size, Merck Millipore).

Derivatisation of ChR2 with MTSL

The cysteines of ChR2 variants were labeled overnight at pH 6 and 4°C with 20 times molar excess of MTSL in buffer containing 20 mM MES, 100 mM NaCl, 0.2% DM. Non-reacted label was removed by washings on Amicon concentrators. To determine the labelling efficiency, both samples were measured in *cw*-EPR against a TEMPOL standard sample of known concentration. Even after careful washing, some remaining free spin label is present in the sample. To separate that signal from the contributions of protein-attached spin label, simulated spectra of free spin label were subtracted from the measured data, allowing for the simultaneous quantification of free spin label content.
Taking into account measurement errors, the lower limits for the resulting labeling efficiencies are >76% for C79 and >73% for C208. The free label content was 6% and 8% respectively.

FTIR difference spectroscopy

Samples used for FTIR spectroscopy were concentrated to 10 mg/ml ChR2 in an aqueous solution of 20 mM MES at pH 6.0. and 2% DM. For time-resolved FTIR experiments, approximately 4 µl of a ChR2 solution were dried on top of a BaF_2 window. The protein film was rehydrated with the saturated vapor phase of a glycerol/water mixture (2/8 w/w) [19] and placed into the FTIR spectrometer (Vertex 80v, Bruker, Rheinstetten, Germany). The sample holder was kept at a constant temperature of 5°C by a circulating water bath (Julabo F25). The photoreaction in the IR experiments was induced by illumination for 3 min with an LED operating at 456 nm.

EPR measurements

Pulsed X-Band EPR-measurements were performed at 9.7 GHz on a Bruker BioSpin (Rheinstetten, Germany) Elexsys E680 X-Band spectrometer, using a Bruker SuperX-FT microwave bridge and Bruker ER 4118X-MD5 dielectric ring resonator. Microwave amplification for pulsed experiments was achieved with an Applied Systems Engineering 117X traveling wave tube amplifier. For ELDOR experiments the E680 spectrometer was equipped with a Bruker E580-400U microwave source. *cw*-EPR experiments were performed on a home-built X-Band spectrometer, using a microwave bridge ER 041 MR, microwave controller ER 048 R, magnet power supply ER 081 S and field controller BH 15, and Super-HQ cavity resonator, all from Bruker. For signal detection a Stanford Research SR810 lock-in detector (Stanford Research Systems, Inc., Sunnyvale, CA, USA) was used. For pELDOR, the four pulse DEER sequence [7] (Probe pulse sequence $\pi/2 - \tau \square - \pi - \tau \square - \tau_2 - \pi - \tau_2$ - echo with the microwave pump pulse on the second frequency being swept between the second and third probe pulse) with pulse lengths of 80 ns for both the $\pi/2$ and the π pulses was used. The relatively long pulses were used to suppress nuclear modulations, since nuclear modulation averaging proved to be inadequate and full suppression of nuclear modulation artifacts was paramount for detecting the presence or absence of short distances in the 1.5 nm range. All *cw*-EPR measurements were performed at room temperature. Low temperatures for pulsed experiments were reached with Oxford CF-935 cryostats (Oxford Instruments, Oxfordshire, United Kingdom). The temperature was controlled using an Oxford ITC503 temperature

controller. A temperature of 40 K was found to yield the best signal-to-noise ratio for ELDOR experiments. For light activation the samples were illuminated with 460 nm light for 3 minutes at 4°C and then rapidly frozen (for pELDOR experiments) or immediately transferred into the spectrometer and measured (for *cw*-experiments).

Analysis

All data analysis was performed in MatLab (The MathWorks Inc., Natick, Mass., USA). For the evaluation of ELDOR data the MatLab toolbox DeerAnalysis [20] was used. Label geometry simulations were performed in MMM [21].

Results and Discussion

Two variants were designed for the pELDOR measurements, one with all cysteines exchanged except C79 (ChR2-C79), and one in which C79 and C208 were left (ChR2-C79/C208). For both variants the cysteine residues were replaced by alanines except C128 which was substituted by threonine. ChR2-C79 shows expression levels comparable to wild-type ChR2, the expression level of ChR2-C79/208 was 4 times higher.

As depicted in Fig. 1, both cysteines are at the intracellular surface of this integral membrane protein. The distance between both cysteines is about 19 Å as derived from the crystallographic structure of chimeric C1C2. As has been previously reported [16,17], replacement of cysteine at position 128 by threonine (C128T) leads to slow photocycling phenotypes. The lifetime of the photocycle intermediate P_3^{520} is prolonged by several orders of magnitude leading to the predominance of the P_3^{520} state under photostationary conditions [19]. The P_3^{520} state was shown to be the open (conducting) state of ChR2. Although the amino acid exchange in the retinal binding pocket of ChR2 leads to complex alterations in the photoreaction of the C128T mutant, the prolonged lifetime of P_3^{520} after illumination and the predominance of the P_3^{520} state under photostationary conditions makes this variant well suited to study the conducting/open state of the ion channel [22].

To check for a potential influence of the mutations on the structural changes of ChR2, FTIR spectroscopy was performed. IR difference spectra of both variants (unlabeled and MTSL labeled) were recorded in the dark state and under photo-stationary conditions after 3 min illumination (456 nm) at 278 K conditions identical to the EPR experiments presented below. Positive bands indicate vibrations in the intermediate state after illumination which are not present in the dark state whereas negative bands are due to vibrations in the dark state, which are not observed in the intermediate state. The difference spectra of the ChR2-C79 (Fig. 4 in supporting information) and ChR2-C79/C208 variants (Fig. 2) share the same prominent features that are observed in the C128T variant [4]. Large amide I difference bands at 1662(-) / 1625(+) cm^{-1} point to substantial alterations in the protein backbone conformation. The negative band at 1554 cm^{-1} was assigned to the C=C double bond stretching vibration of the retinal chromophore in the ground state which shifts to 1533 cm^{-1} in the accumulated P_3^{520} state. The fingerprint region shows a positive band at 1180 cm^{-1} which indicates the presence of 13-cis retinal with protonated Schiff base. These retinal vibrations suggest predominant accumulation of P_3^{520}. In conclusion, the strong similarity of the light-induced IR difference spectra of the ChR2-C79 and ChR2-C79/C208 variants in comparison to the C128T variant suggests identical functionality. Also, there are no indications for an influence of the bound spin label on the structural changes of ChR2 as detected by FTIR spectroscopy.

To observe light dependent changes of ChR2, *cw*-EPR spectra at room temperature and pELDOR traces at 50K were recorded for each sample in the dark as well as after illumination. Samples were illuminated under identical conditions to those used for FTIR spectroscopy

before being transferred directly to the spectrometer (for *cw* experiments) or rapidly frozen (for ELDOR spectroscopy).
cw-spectra show that in the dark state the label at C79 is mostly rigidly attached to the protein while the label at C208 shows a greater degree of mobility (Fig. 5 in supporting information). Although we could detect a slight increase in mobility for C79 upon light activation, the differences in the *cw*-spectra between the dark and the light state are insignificant. Furthermore, neither the *cw*-EPR spectra of ChR2-C79 nor of ChR2-C79/C208 show significant broadening. Additional low temperature X-Band EPR spectra do not show dipolar broadening either, leading to the conclusion that there are no interacting close spin pairs present.

pELDOR spectroscopy was utilized to quantify inter-spin distances. To ensure a proper fit of the background, data sets were created by combining a short (1.4 µs), high-resolution, low-noise 4pDEER time trace for the initial decay with a long (2.8 µs), low-resolution 4pDEER trace for background determination. The data was then phase- and background corrected using a three dimensional homogeneous spin distribution. Spin distance distributions were then obtained by using the DeerAnalysis program [20], employing Gaussian distributions to minimize the risk of producing spurious resolution. A comparison of this approach to the more standard Tikhonov regularization method is shown in the supporting information (Fig. 6). To stabilize the fit for long dipolar evolution times it was necessary to treat the data with a hamming window to prevent background noise from adversely affecting the fit (Fig. 3a, 3c).
The pELDOR time trace of the spin-labeled ChR2-C79 variant (Fig. 3a) shows a fast decay of the signal intensity within the first 500 ns which is unexpected for a monomeric protein with a single spin-label. The distance distribution derived from the time trace displays a sharp peak at 3.7 nm (Fig. 3b) proving that this ChR2 mutant forms a dimer under our conditions. The C79-C79 distance is well resolved even though it lacks C34 and C36 reported to stabilize dimerization by bridging the monomers with disulfide bonds [6]. Additionally, a broad background distribution between 2 and 7 nm is observed, most likely due to aggregation of the protein. The 3.7 nm distance between the spin labels at C79 in the dimeric protein is slightly larger than the 3.3 nm average distance predicted by the MMM program [21] but is still in agreement with the C1C2 chimera structure [6] considering the flexibility of the spin label. Upon blue-light activation, the low noise part of the time trace clearly shows a slower signal decay together with a loss of the oscillation. This is reflected in the distance distribution by a shift of the maximum by 0.5 nm to 4.2 nm together with significant broadening. The distance distribution at distances larger than 5 nm is not altered after illumination, indicating that this part is indeed not due to a specific C79-C79 interaction, but rather aggregation.
The dimeric arrangement of ChR2 yields 4 interacting spins present in the ChR2-C79/C208 variant with 4 nonequivalent pair distances. This severely complicates the interpretation of the pELDOR data. However, the low noise part of the time trace (Fig. 3c) already shows a change between the open and closed states as in the case for ChR2-C79. The slower decay of the signal in the open state again indicates a distance increase between the labels compared to the closed state. The oscillation visible in the dark state time trace for ChR2-C79 is absent in ChR2-C79/C208. Correspondingly, the narrow signal from C79-C79 in ChR2-C79 in the closed state is no longer discernible in the distance distribution for the ChR2-C79/C208 variant (Fig. 3d). Significant distance contributions appear in this case already in the 2.5 nm range. Such short distances are expected for the C79-C208 intra-monomer pair based on the C1C2 chimera structure [6], while distances in the 4 nm range are expected for the C79-C208 inter-monomer pairs, overlaying the signal already identified as arising from C79-C79. Further distances in the 5 nm range are expected from the C1C2 chimera structure [6] for the C208-C208 pair and are visible as significant intensity of the distance distribution in this range. The maximum position of the distance distribution in the dark state is shifted compared to the distance observed in ChR2-C79 (4.0 nm vs. 3.7 nm, respectively), consistent with the expected additional distances

in the 4 nm range for the C79-C208 intra-monomer pairs. These additional distance contributions explain the lack of a visible oscillation in the ChR2-C79/C208 dark state time trace. The maximum position again exhibits a distinct shift to larger distances upon light-activation (by 0.4 nm). Interestingly, both inflection points of the distance distribution also shift to larger distances. The inflection point on the short distance side moves by about 0.15 nm to larger distances, while that on the long distance side shifts from 5.2 nm in the closed to 5.4 nm in the open state. The overall shift of the distance distribution is consistent with an increase of the intra-monomer C79-C208 distance, the inter-monomer C79-C208 distance pair as well as the C208-C208 inter-monomer distance.

According to the crystallographic structure of the C1C2 chimera [6], helix F is located remote from the dimerization interface (see Fig. 1) and a movement of helix F alone should only affect the C79-C208 and C208-C208 distances. In agreement with EPR experiments on BR and SRII [10-12], we find changes in distances involving C208 in the F helices. However in addition, we also find considerable changes in the ChR2-C79 variant, which cannot be solely attributed to the movement of helix F. Therefore, the C79-C79 distance changes reflect additional structural changes either in the dimerization interface or involving helix B which is adjacent to C79. A movement of helix B was also observed for BR in the purple membrane using 2D diffraction experiments with neutrons [23], X-rays [24-26] and electrons [27]. Such conformational changes are induced by retinal isomerization which triggers transient protonation changes of the retinal Schiff base and internal amino acid side chains (D253, D156 and E90) as recently shown by time-resolved FTIR difference spectroscopy [28]. The large conformational changes of the protein backbone lead to the transient influx of water molecules, which tally the onset of cation permeation. Despite the fact that the lateral arrangement of the transmembrane α-helices is different in ChR2 as compared to other microbial rhodopsins, the changes in tertiary structure seem to be conserved. EPR experiments on ChR2 spin labeled at other sites will help elucidating further details of structural changes that accompany channel opening and closure.

Acknowledgements

We thank Dorothea Heinrich for excellent technical assistance. This work was supported by the Deutsche Forschungsgemeinschaft, SFB 1078, projects B3 and B4.

References

[1] Nagel, G.; Szellas, T.; Huhn, W.; Kateriya, S.; Adeishvili, N.; Berthold, P.; Ollig, D.; Hegemann, P.; Bamberg, E. (**2003)** Channelrhodopsin-2, a directly light-gated cation-selective membrane channel. *P. Natl. Acad. Sci. USA, 100(24)*, 13940–13945.

[2] Zhang, F.; Aravanis, A. M.; Adamantidis, L., A.and de Lecea; Deisseroth, K. (**2007)** Circuit-breakers: optical technologies for probing neural signals and systems. *Nat. Rev. Neurosci., 8(9)*, 577–581.

[3] Ritter, E.; Stehfest, K.; Berndt, A.; Hegemann, P.; Bartl, F. J. (**2008)** Monitoring Light-induced Structural Changes of Channelrhodopsin-2 by UV-visible and Fourier Transform Infrared Spectroscopy. *J. Biol. Chem, 283(50)*, 35033–35041.

[4] Radu, I.; Bamann, C.; Nack, M.; Nagel, G.; Bamberg, E.; Heberle, J. *(***2009)** Conformational Changes of Channelrhodopsin-2. *J. Am. Chem. Soc., 131(21)*, 7313–7319.

[5] Nack, M.; Radu, I.; Schultz, B. J.; Resler, T.; Schlesinger, R.; Bondar, A. N.; del Val, C.; Abbruzzetti, S.; Viappiani, C.; Bamann, C.; Bamberg, E.; Heberle, J. *(***2012)** Kinetics of proton release and uptake by channelrhodopsin-2. *FEBS Lett., 586(9)*, 1344–1348.

[6] Kato, H. E.; Zhang, F.; Yizhar, O.; Ramakrishnan, C.; Nishizawa, T.; Hirata, K.; Ito, J.; Aita, Y.; Tsukazaki, T.; Hayashi, S.; Hegemann, P.; Maturana, A. D.; Ishitani, R.; Deisseroth, K.; Nureki, O. (**2012)** Crystal structure of the channelrhodopsin light-gated

cation channel. *Nature*, *482(7385)*, 369–374.
[7] Martin, R. E.; Pannier, M.; Diederich, F.; Gramlich, V.; Hubrich, M.; Spiess, H. W. *(***1998)** Determination of end-to-end distances in a series of TEMPO diradicals of up to 2.8 nm length with a new four-pulse double electron electron resonance experiment. *Angew. Chem. Int. Edit.*, *37(20)*, 2834–2837.
[8] Altenbach, C.; Kusnetzow, A. K.; Ernst, O. P.; Hofmann, K. P.; Hubbell, W. L. (**2008)** High-resolution distance mapping in rhodopsin reveals the pattern of helix movement due to activation. *Proc. Natl. Aca. Sci. USA*, *105(21)*, 7439–7444.
[9] Steinhoff, H. J.; Mollaaghababa, R.; Altenbach, C.; Hideg, K.; Krebs, M.; Khorana, H. G.; Hubbell, W. L. (**1994)** Time-resolved detection of structural changes during the photocycle of spin-labeled bacteriorhodopsin. *Science*, *266(5182)*, 105–107.
[10] Wegener, A. A.; Chizhov, I.; Engelhard, M.; Steinhoff, H. J. Time-resolved detection of transient movement of helix F in spin-labelled pharaonis sensory rhodopsin II. (**2000)** *J. Mol. Biol.*, *301(4)*, 881–891.
[11] Klare, J. P.; Bordignon, E.; Engelhard, M.; Steinhoff, H. J. *(***2004)** Sensory rhodopsin II and bacteriorhodopsin: Light activated helix F movement. *Photochem. Photobio. Sci.*, *3(6)*, 543–547.
[12] Wegener, A. A.; Klare, J. P.; Engelhard, M.; Steinhoff, H. J. (**2001)** Structural insights into the early steps of receptor-transducer signal transfer in archaeal phototaxis. *EMBO J.*, *20(19)*, 5312–5319.
[13] Resek, J. F.; Farahbakhsh, Z. T.; Hubbell, W. L.; Khorana, H. G. (**1993)** Formation of the meta-II photointermediate is accompanied by conformational changes in the cytoplasmic surface of rhodopsin. *Biochemistry*, *32(45)*, 12025–12032.
[14] Kusnetzow, A. K.; Altenbach, C.; Hubbell, W. L. (**2006)** Conformational states and dynamics of rhodopsin in micelles and bilayers. *Biochemistry*, *45(17)*, 5538–5550.
[15] Knierim, B.; Hofmann, K. P.; Ernst, O. P.; Hubbell, W. L. Sequence of late molecular events in the activation of rhodopsin. *Proc. Natl. Aca. Sci. USA* **2007**, *104*, 20290–20294.
[16] Berndt, A.; Yizhar, O.; Gunaydin, L. A.; Hegemann, P.; Deisseroth, K. *(***2009)** Bi-stable neural state switches. *Nat. Neurosci.*, *12(2)*, 229–234.
[17] Bamann, C.; Gueta, R.; Kleinlogel, S.; Nagel, G.; Bamberg, E. (**2010)** Structural Guidance of the Photocycle of Channelrhodopsin-2 by an Interhelical Hydrogen Bond. *Biochemistry*, *49(2)*, 267–278.
[18] Bamann, C.; Kirsch, T.; Nagel, G.; Bamberg, E. *(***2008)** Spectral characteristics of the photocycle of channelrhodopsin-2 and its implication for channel function. *J. Mol. Biol.*, *375(3)*, 686–649.
[19] Noguchi, T.; Sugiura, M. *(***2002)** Flash-induced FTIR difference spectra of the water oxidizing complex in moderately hydrated photosystem II core films: Effect of hydration extent on S-state transitions. *Biochemistry*, *41(7)*, 2322–2330.
[20] Jeschke, G.; Chechik, V.; Ionita, P.; Godt, A.; Zimmermann, H.; Banham, J.; Timmel, C. R.; Hilger, D.; Jung, H. *(***2006)** DeerAnalysis2006 - a comprehensive software package for analyzing pulsed ELDOR data. *Appl. Magn. Reson.*, *30(3-4)*, 473–498.
[21] Polyhach, Y.; Bordignon, E.; Jeschke, G. *(***2011)** Rotamer libraries of spin labelled cysteines for protein studies. *Phys. Chem. Chem. Phys.*, *13(6)*, 2356–2366.
[22] Ritter, E.; Piwowarski, P.; Hegemann, P.; Bartl, F.J. (**2013)** Light-dark Adaptation of Channelrhodopsin C128T Mutant. *J. Biol. Chem.*, *288(15)*, 10451-10458.
[23] Dencher, N. A.; Dresselhaus, D.; Zaccai, G.; Buldt, G. (**1989)** Structural changes in bacteriorhodopsin during proton translocation revealed by neutron diffraction. *P. Natl. Acad. Sci. USA*, *86(20)*, 7876-7879.
[24] Koch, M. H. J.; Dencher, N. A.; Oesterhelt, D.; Plohn, H. J.; Rapp, G.; Buldt, G. (**1991)** Time-resolved X-ray diffraction study of structural changes associated with the

photocycle of bacteriorhodopsin. *EMBO J.*, *10(3)*, 521-526.
[25] Nakasako, M.; Kataoka, M.; Amemiya, Y.; Tokunaga, F. (**1991)** Crystallographic characterization by X-ray diffraction of the M-intermediate from the photo-cycle of bacteriorhodopsin at room-temperature. *FEBS Lett.*, *292(1-2)*, 73-75.
[26] Sass, H. J.; Schachowa, I. W.; Rapp, G.; Koch, M. J. H.; Oesterhelt, D.; Dencher, N. A.; Buldt, G. (**1997)** The tertiary structural changes in bacteriorhodopsin occur between M states: X-ray diffraction and Fourier transform infrared spectroscopy. *EMBO J.*, *16(7)*, 1484-1491.
[27] Subramaniam, S.; Gerstein, M.; Oesterhelt, D.; Henderson, R. (**1993)** Electron-diffraction analysis of structural changes in the photocycle of bacteriorhodopsin. *EMBO J.*, *12(1)*, 1-8.
[28] Lorenz-Fonfria, V. A.; Resler, T.; Krause, N.; Nack, M.; Gossing, M.; Fischer von Mollard, G.; Bamann, C.; Bamberg, E.; Schlesinger, R.; Heberle, J. (**2013)** Transient protonation changes in channelrhodopsin-2 and their relevance to channel gating. *P. Natl. Acad. Sci. USA*, *110(14)*, E1273-1281.

Figures

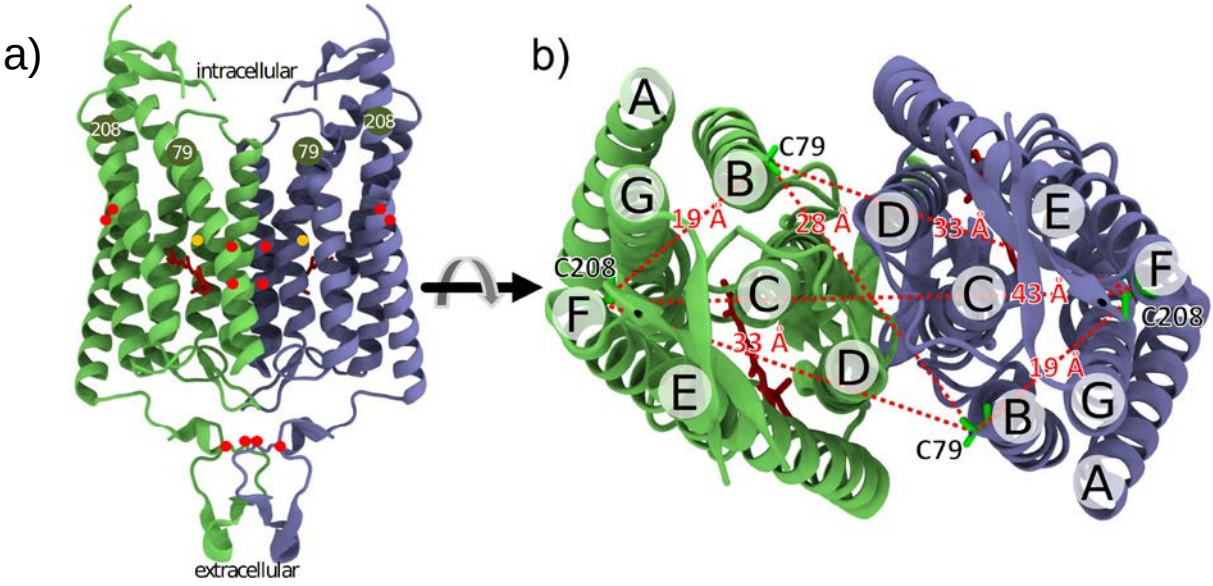

Figure 1. ChR1/ChR2 chimera structure (PDB: 3UG9). The dimer assembly was generated with PISA.[19] a) side view: Circles show the position of cysteines from an sequence alignment with ChR2 [6]. Red/yellow dots indicate cysteines in the ChR2-C79/C208 variant exchanged for alanine/threonine. Green circles indicate the residual cysteines in this variant. b), view from cytoplasm: Distances between the C_α-atoms of cysteine 79 and 208 are depicted with red dashed lines.

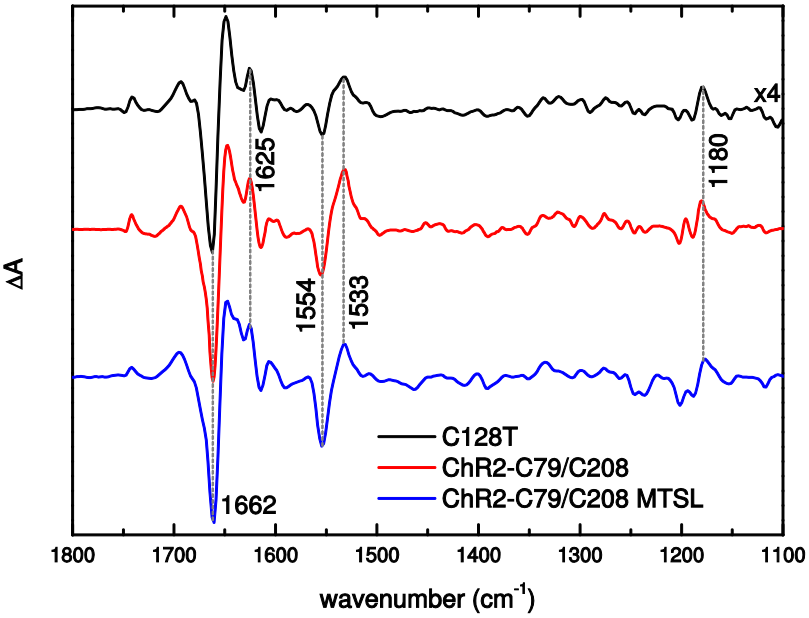

Figure 2. Light-induced FTIR difference spectra of ChR2 variants C128T (black) and ChR2-C79/C208 unlabeled (red) and MTSL labeled (blue). The spectra were recorded under photostationary conditions (after 3 min illumination, 456 nm) at 278 K. The spectrum of the C128T variant was taken from Radu *et al*. [4].

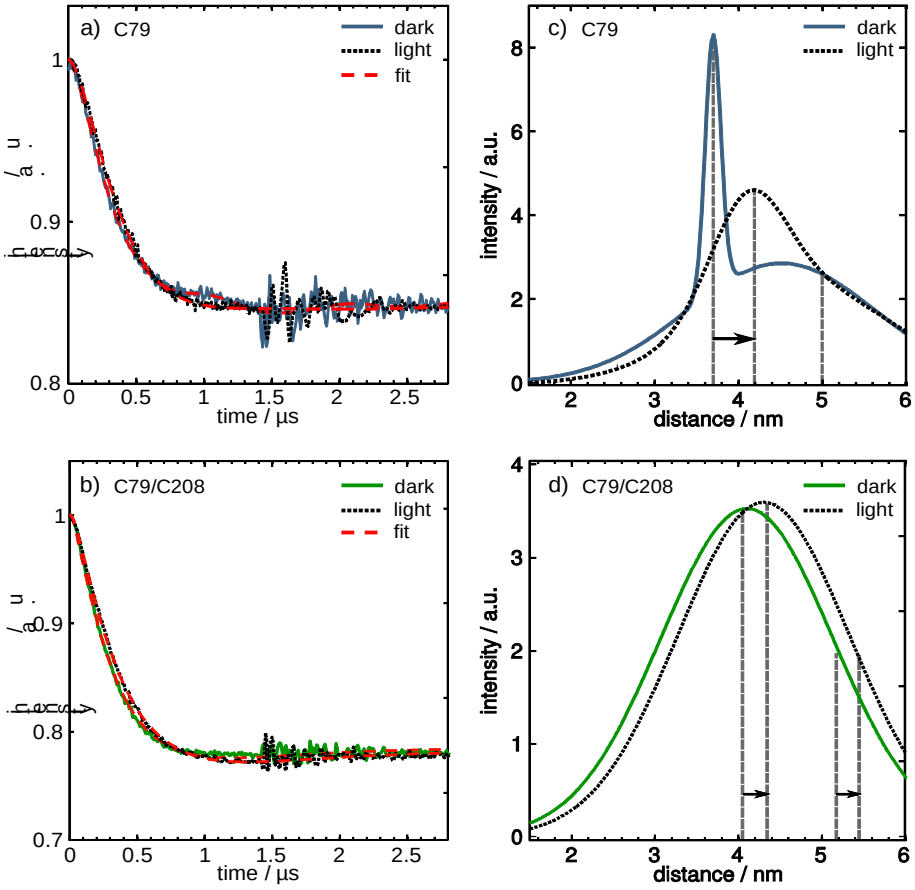

Figure 3. Left column: Background-corrected pELDOR measurements of ChR2 labeled at C79 (a) and C79/C208 (b) in dark and light state. For each data set two pELDOR measurements of different length were combined, the resulting trace was treated with a hamming window after background correction to stabilize the fit. Right column: Distance distributions of C79- (c) and C79/C208-labeled (d) ChR2. ChR2-C79 shows a broad background with a sharp feature at 3.7 nm that shifts to 4.2 nm upon light activation. A similar shift occurs in ChR2-C79/C208, with an additional shift of the distribution's inflection point from 5.2 nm to 5.4 nm.

Supporting Information

Additional figures

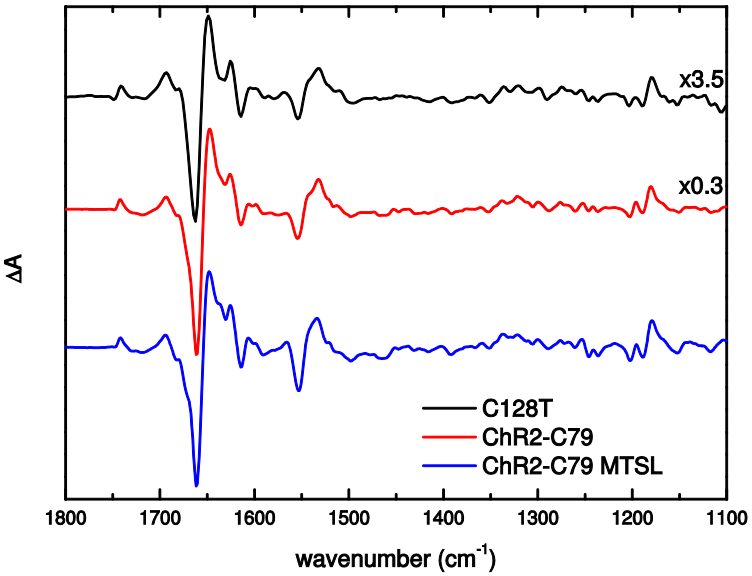

Figure 4. Light-induced FTIR difference spectra of ChR2 variants C128T (black) and ChR2-C79 unlabeled (red) and MTSL labeled (blue). The spectra were recorded under photostationary conditions (after 3 min illumination, 456 nm) at 278 K. The spectrum of the C128T variant is taken from Radu *et al.* [1].

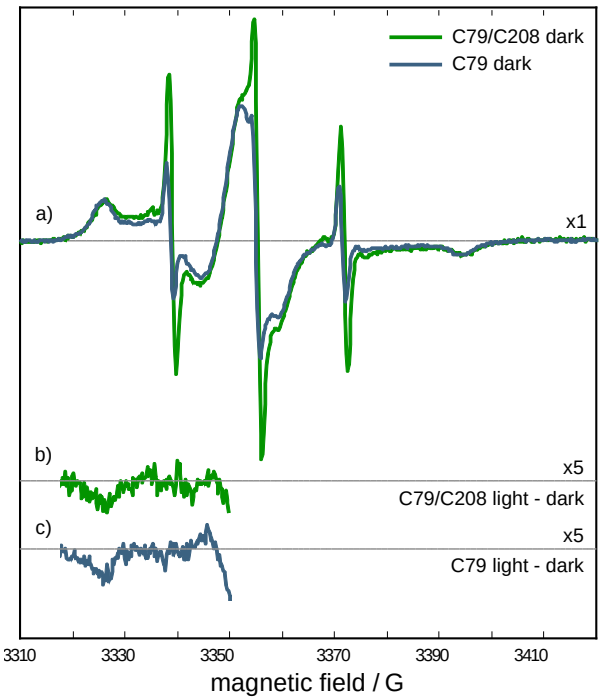

Figure 5. *cw*-spectra recorded at room temperature of ChR2-C79 and ChR2-C79/C108. The sharp peaks at 3325 G and 3395 are due to the label at C79 and indicates that this label is rigidly bound to the backbone. The label at C208 is visible as an increase in signal intensity between 3330 G and 3390 G, indicating that this label is much more flexibly bound. b) and c): five-fold magnification of difference spectra light–dark for ChR2-C79/C208 (b) and ChR2-C79 (c). While a slight change in the mobility of the label at C79 is visible, this effect is negligible.

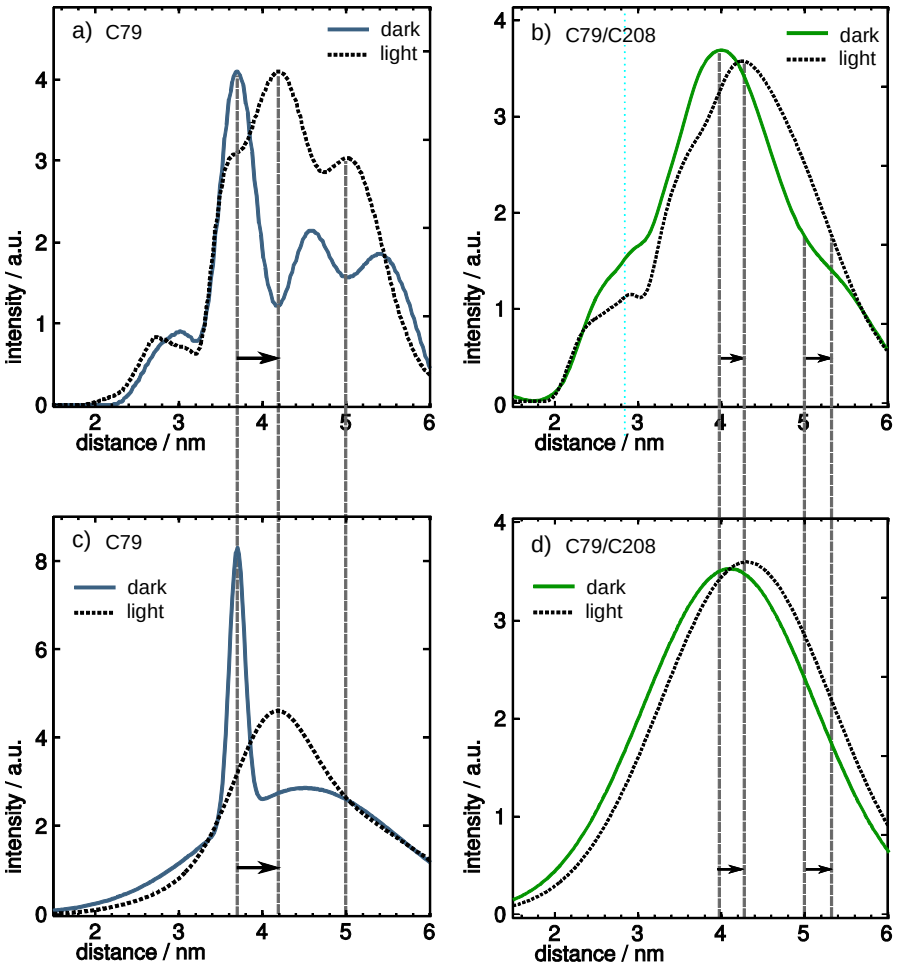

Figure 6: Comparison of distance distribution fitting using Tikhonov regularisation (a,b) and gaussian curves (c,d) for ChR2-C79 and ChR2-C79/C208, respectively. Both the Tikhonov and the gaussian model agree well regarding the dominant shifts in distance distributions.